JCB Article

Fascin-mediated propulsion of *Listeria monocytogenes* independent of frequent nucleation by the Arp2/3 complex

William M. Brieher, Margaret Coughlin, and Timothy J. Mitchison

Department of Systems Biology, Harvard University Medical School, Boston, MA 02115

Actin-dependent propulsion of *Listeria monocytogenes* is thought to require frequent nucleation of actin polymerization by the Arp2/3 complex. We demonstrate that *L. monocytogenes* motility can be separated into an Arp2/3-dependent nucleation phase and an Arp2/3-independent elongation phase. Elongation-based propulsion requires a unique set of biochemical factors in addition to those required for Arp2/3-dependent motility. We isolated fascin from brain extracts as the only soluble factor required in addition to actin during the elongation phase for this type of movement. The nucleation reaction assembles a comet tail of branched actin filaments directly behind the bacterium. The elongation-based reaction generates a hollow cylinder of parallel bundles that attach along the sides of the bacterium. Bacteria move faster in the elongation reaction than in the presence of Arp2/3, and the rate is limited by the concentration of G-actin. The biochemical and structural differences between the two motility reactions imply that each operates through distinct biochemical and biophysical mechanisms.

Introduction

The actin cytoskeleton is a system of proteins that can perform mechanical work. In some situations, myosin motors generate the force to perform work while actin filaments provide directional tracks for myosin translocation. In others, actin polymerization itself appears to perform mechanical work. New actin polymer can be generated by creating a filament de novo from G-actin subunits in a process referred to as nucleation. Alternatively, new polymer can be generated by extending existing filaments, which we refer to as elongation.

The frequency of nucleation is an important factor in determining the morphology of actin-based cellular structures (Svitkina and Borisy, 1999; Svitkina et al., 2003; Vignjevic et al., 2003) It may also influence the force producing mechanisms entailed in these structures. For example, nucleation is frequent in protruding sheets termed lamellipodia (Theriot and Mitchison, 1991) where actin filaments are typically short and organized in dendritic branches (Svitkina and Borisy, 1999). Nucleation is less frequent in protruding cylinders such as filopodia where new polymer may be formed solely through elongation of existing filaments (Mallavarapu and Mitchison, 1999), and in these structures filaments are organized into parallel bundles (Lewis and Bridgman, 1992; Svitkina et al., 2003). Although protrusion of lamellipodia (Theriot and Mitchison, 1991) and filopodia (Mallavarapu and Mitchison, 1999) are tightly coupled to actin polymerization, the distinct organization and generation of actin filaments in each structure raises the possibility that each might use a different mechanism to produce mechanical force.

Progress on the mechanism by which actin polymerization can perform mechanical work has been facilitated by the discovery that a number of intracellular pathogens, including *Listeria monocytogenes*, propel themselves through the host cytoplasm by assembling an actin comet tail that grows at the tail–bacterial interface (Cameron et al., 2000; Portnoy et al., 2002). This motility mechanism is probably similar to rocketing of endocytic vesicles (Taunton et al., 2000), and shares biochemistry with leading edge structures (Pollard and Borisy, 2003). Like lamellipodial protrusion, *L. monocytogenes* motility is thought to be driven by frequent, Arp2/3-dependent nucleation that generates a tail containing short, highly branched filaments (Tilney and Portnoy, 1989; Theriot et al., 1992). Reconstitution of *L. monocytogenes* motility in a

Address correspondence to William M. Brieher, Dept. of Systems Biology, Harvard University Medical School, 250 Longwood Ave., SGM-523, Boston, MA 02115. Tel.: (617) 432-3724. Fax: (617) 432-3702. email: bill_brieher@hms.harvard.edu

Key words: actin; Arp2/3; fascin; filopodia; *Listeria*

Abbreviations used in this paper: AMPPNP, adenosine 5′-(β,γ-imido)triphosphate; β-Me, β-mercaptoethanol; CA; cofilin homology and acidic region of N-WASP; Ptk, rat kangaroo kidney; TMR, tetramethylrhodamine.

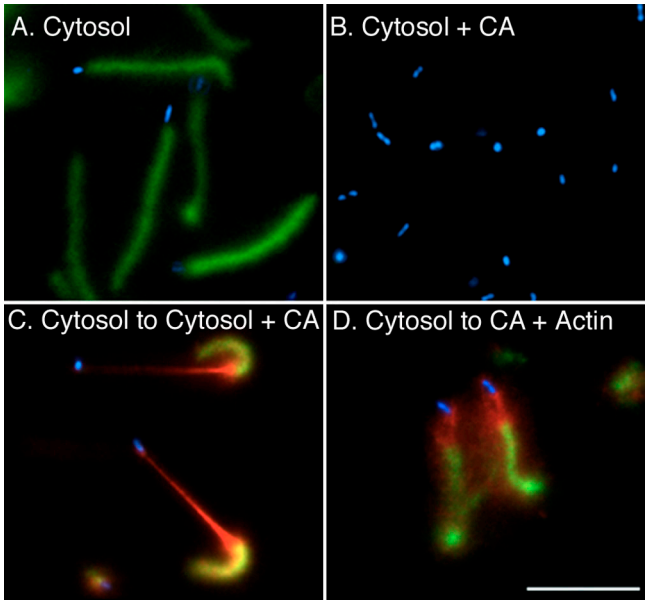

Figure 1. ***Listeria* motility continues in the absence of Arp2/3-mediated nucleation.** Bacteria are labeled blue and actin is green or red. (A) *Listeria* moving in brain cytosol. (B) *Listeria* in cytosol containing the Arp2/3 inhibitor CA. (C) *Listeria* moving initially in cytosol and Alexa® 488–labeled actin (green), then switched to cytosol containing CA and TMR-labeled actin (red). (D) As per C, but then switched to CA and TMR-labeled actin alone. Bar, 10 μm (applies to all panels).

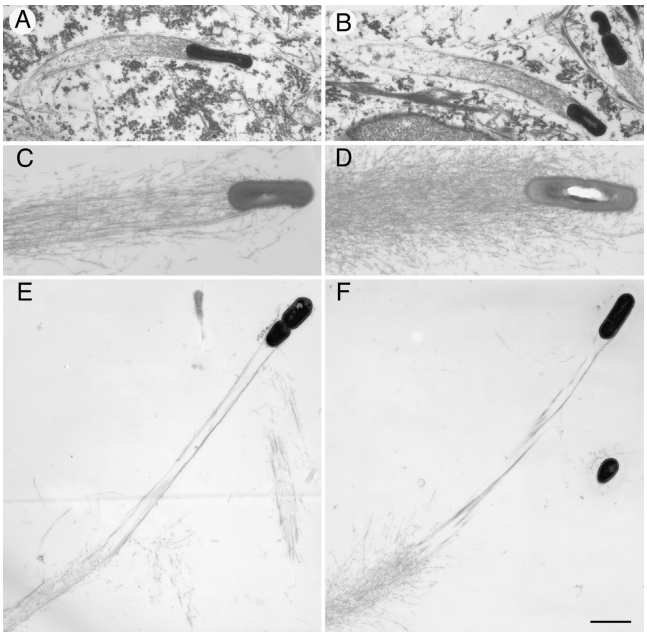

Figure 2. **Actin comet tails consist of branched filaments and parallel bundles.** Thin-section EM of *L. monocytogenes* comet tails in infected PtK cells (A and B), brain cytosol that produces a comet tail consisting of branched filaments and parallel bundles (C), and brain cytosol that produces only branched filaments (D). (E) Comet tails formed initially in brain cytosol that forms branched and bundled filaments, then switched to the same cytosol containing CA. (F) Comet tails formed initially in brain cytosol that forms only branched filaments, then switched to the same cytosol containing CA. Bars: (A, B, E, and F) 1 μm; (C and D) 0.75 μm.

biochemically defined system (Loisel et al., 1999) has permitted detailed investigation of the biochemical and biophysical mechanism coupling polymerization with frequent nucleation to mechanical force production (Bernheim-Groswasser et al., 2002; Wiesner et al., 2003). We currently lack a similarly tractable reconstituted system for dissecting the mechanism for force production by elongation-dominated structures like filopodia. Here, we show that *L. monocytogenes* can move in the absence of frequent nucleation and begin the biochemical and structural characterization of this form of motility.

Results

L. monocytogenes motility initiates from an actin cloud whose formation requires actin nucleation by the Arp2/3 complex (Welch et al., 1997; May et al., 1999; Yarar et al., 1999). To test if motility continues to require Arp2/3 activity after cloud nucleation, motility assays were performed in perfusion chambers. Motility could then be dissected into two steps: tail nucleation and tail elongation. We used actin tagged with different fluorophores to reveal the step during which a given segment of the comet tail polymerized. Motility was initiated with cytosol containing Arp2/3 and green actin. This solution was then replaced with cytosol containing an Arp2/3 inhibitor and red actin. We used the cofilin homology and acidic region of N-WASP (CA) domain of N-WASP to inhibit Arp2/3. This domain binds Arp2/3 and competitively inhibits binding of Arp2/3 activators including the ActA protein of *L. monocytogenes* (May et al., 1999). Bacteria mixed with brain cytosol formed comet tails (Fig. 1 A). Addition of CA to cytosol inhibited all actin polymerization around the bacteria (Fig. 1 B). However, once Arp2/3 initiated motility, its activity was no longer required for comet tail assembly. Motility in the absence of Arp2/3-driven nucleation was evident from an additional segment of comet tail containing red actin after the initiating cytosol was replaced with cytosol containing CA (Fig. 1 C). The segment of tail formed by elongation in cytosol, CA, and red actin appeared thinner, stiffer, and less fuzzy than the initial tail formed with active Arp2/3. Replacing the initiating cytosol with CA and actin alone resulted in only a short stretch of newly assembled actin (Fig. 1 D). Therefore, after initiation by Arp2/3, comet tails continue to assemble in its absence in a reaction that requires cytosolic factors in addition to actin.

Actin filament arrays assembled by Arp2/3-dependent nucleation are characterized by their highly branched, dendritic organization (Mullins et al., 1998; Svitkina and Borisy, 1999; Cameron et al., 2001). We used EM to visualize actin filament organization in comet tails assembled in the presence or absence of Arp2/3-nucleating activity (Fig. 2). For comparison, we first looked at the structure of *L. monocytogenes* comet tails in infected rat kangaroo (PtK) cells (Fig. 2, A and B). Comet tails assembled in vivo appeared to consist of two populations of actin filaments. A dendritic network of highly branched filaments is ensheathed by a cylinder of bundles running parallel to the direction of movement. Comet tails assembled by *L. monocytogenes* moving in brain extracts

fell into two different classes. One class contained both filament organizations with prominent bundles surrounding a branched interior network (Fig. 2 C). The other class consisted almost exclusively of the branched filaments (Fig. 2 D). The type of comet tail that forms is extract dependent. Of six different brain extracts, two extracts primarily formed the hybrid tail consisting of branched as well as parallel bundles of filaments, as shown in Fig. 2 C (24/28 comet tails examined contained both filament organizations, whereas the remaining four comet tails contained only branched filaments). The other four extracts formed comet tails consisting primarily of branched filaments, as shown in Fig. 2 D (67/67 comet tails examined). We do not know the source of the variability between cytosolic extracts. In the two-step reaction, we observed an abrupt structural change between the portion of the tail generated in cytosol alone and that generated in cytosol + CA (Fig. 2, E and F). This structural change was independent of the type of comet tail formed in step 1. The first part contains branched filaments, whereas the second part consists only of long bundles running parallel to the direction of movement. The bundles are still arranged into a cylinder, but now the interior is largely hollow. If the first portion of the comet tail consisted of both branched filaments and parallel bundles, the bundles in the second portion appeared to extend off the original bundles (Fig. 2 E; 11/11 examined). If the first portion of the comet tail consisted solely of branched filaments, they were stitched together into parallel bundles in step 2 (Fig. 2 F; 23/23 examined) in a manner analogous to bundle formation from a dendritic network described by Vignjevic et al. (2003). This structural transition within comet tails is also quite similar to that seen after addition of G-actin to detergent-extracted infected cells (Tilney et al., 1992), suggesting that our assay might be reporting on the same activity as that seen in the Tilney work. From our EM, we conclude that continued assembly of the branched network in the center of the tail requires Arp2/3 nucleation, whereas the sheath of parallel bundles can apparently elongate independent of frequent nucleation by Arp2/3.

Arp2/3-dependent *L. monocytogenes* motility has been reported with seven pure proteins (Loisel et al., 1999). We wished to identify the biochemical factors required for Arp2/3-independent motility. We were unable to reconstitute Arp2/3-independent motility using mixtures of known factors, and a direct fractionation approach quickly resulted in the loss of all activity even when fractions were mixed with known factors. This suggested that Arp2/3-independent motility requires more than one new factor. Therefore, to facilitate its biochemical dissection, we divided *L. monocytogenes* motility into a set of subreactions in an attempt to make at least one subreaction dependent upon a single factor. We divided *L. monocytogenes* propulsion into three steps (Fig. 3 A). In the first step, *L. monocytogenes* are preincubated in cytosol under conditions that prevent actin polymerization. This allows recruitment of essential factors to the bacterial surface. The second step initiates actin polymerization and motility in the presence of purified Arp2/3, capping protein, and actin. In the third step, the initiating mixture is replaced with actin, CA, and brain fractions to be tested for elongation activity. All three steps are required for Arp2/3-independent propulsion in step 3,

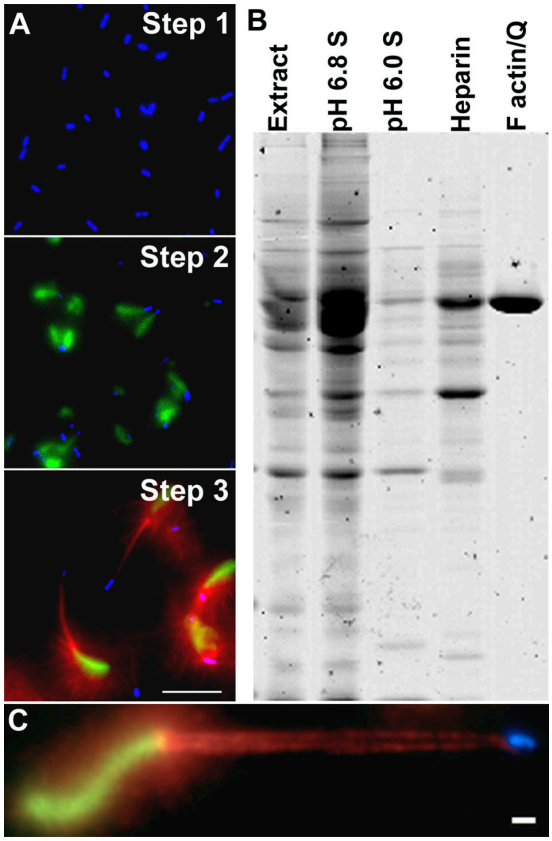

Figure 3. **Isolation of fascin as the only motility factor required in addition to actin for movement in the absence of Arp2/3.** (A) Separation of *Listeria* propulsion into three steps: (step 1) preincubation step in cytosol; (step 2) nucleation phase with Arp2/3, capping protein, and Alexa® 488–labeled actin; and (step 3) elongation phase in CA, TMR-labeled actin, and fascin purified from bovine brain. (B) SDS-PAGE summarizing the purification of fascin using the three-step assay. (C) Result of a three-step assay using bacterially expressed, recombinant fascin in step 3. The comet tail assembled in step 2 (nucleation in Arp2/3) is labeled green, and the portion assembled in step 3 (elongation in fascin) is labeled red. Bars: (A) 5 μm; (C) 1 μm.

and actin alone in step 3 was not sufficient for sustained propulsion.

We fractionated brain extracts to identify the additional factor required in step 3 for persistent motility. A purification scheme from brain cytosol ended with the isolation of a single polypeptide of 56 kD that was identified by mass spectrometry as the actin-bundling protein fascin (Fig. 3 B). Actin + CA + recombinant fascin expressed in bacteria and purified was sufficient, in step 3, to support continued comet tail assembly in the absence of Arp2/3 (Fig. 3 C). We conclude that fascin is the only soluble protein required in addition to actin for Arp2/3-independent motility.

The actin-bundling proteins fimbrin (Kocks and Cossart, 1993) and α-actinin (Dabiri et al., 1990) have been localized to actin comet tails of *L. monocytogenes*. To see if fascin localized to comet tails, *L. monocytogenes*-infected BSC-1 cells and XTC cells were stained for fascin (Fig. 4). Fascin localized to comet tails in both cell types.

We tested other bundling proteins for their ability to substitute for fascin in Arp2/3-independent motility. Reactions

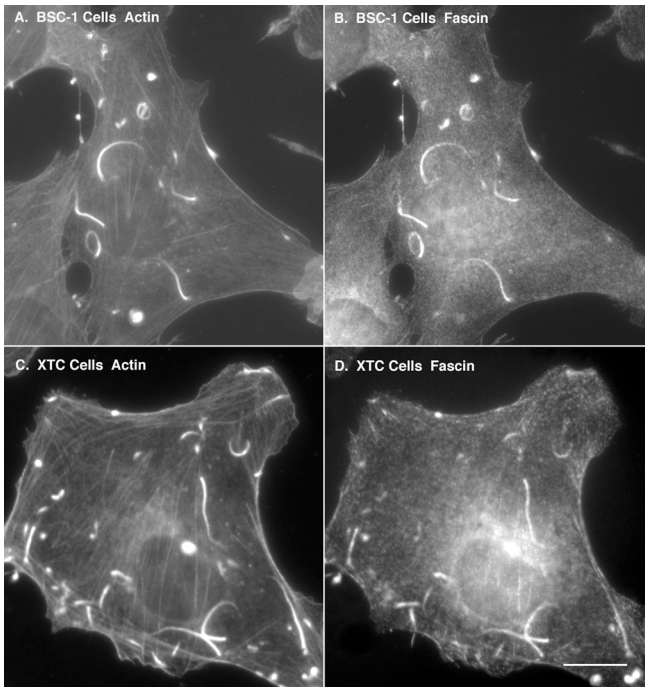

Figure 4. **Fascin localizes to comet tails in *L. monocytogenes*–infected cells.** Infected BSC-1 cells (A and B) or XTC cells (C and D) were costained for actin (A and C) and fascin (B and D). Bar, 10 μm.

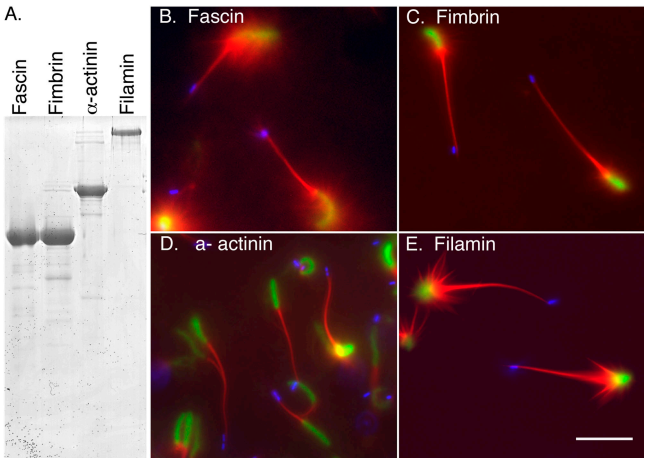

Figure 5. **Different bundling proteins can mediate Arp2/3-independent motility.** (A) Coomassie-stained gel of the bundling proteins used for the elongation reactions. Fascin is a fascin–thioredoxin fusion protein causing it to run at 68 kD. (B–E) Arp2/3-independent motility using either fascin (B), fimbrin (C), α-actinin (D), or filamin (E) in the elongation step. All reactions were performed using the three-step protocol described in Fig. 3. Green actin marks the portion of the comet tail assembled in the presence of Arp2/3. Red actin marks the portion of the comet tail assembled during the elongation phase in the presence of the indicated bundling protein and CA. Bar, 10 μm.

were performed using the three-step protocol described above, but using either fascin, fimbrin, α-actinin, or filamin in step 3 (the elongation step). All of these bundling proteins scored in the reaction when present at 1 μM (Fig. 5). For each bundling protein, ∼30–40% of the bacteria that assembled clouds or comet tails in step 2 elongated in step 3 (for fascin, 68/210; fimbrin, 54/177; α-actinin, 36/91; filamin, 24/83). Therefore, Arp2/3-independent elongation requires bundling of actin filaments, but is not a unique property of fascin.

To gain insight into the biophysical mechanisms involved in propulsion, comet tails assembled under Arp2/3-dependent and -independent conditions were visualized by thin-section EM. Incubating bacteria in Arp2/3 and actin alone resulted in the formation of actin clouds containing highly branched filaments (Fig. 6 A). Bacteria assembled comet tails after preincubation in cytosol in the presence of actin, Arp2/3, and capping protein. Filaments under these conditions are short and highly branched with no bundles or long filaments visible (Fig. 6 B). Filament organization under these conditions matches that seen in the presence of Arp2/3 and actin alone, the main difference being the assembly of a comet tail as opposed to a symmetric cloud. This demonstrates that *L. monocytogenes* moving under these conditions undergo frequent rounds of Arp2/3-mediated nucleation. When the nucleation mix is replaced with fascin, CA, and actin, the organization of the comet tail switches abruptly to bundles of filaments parallel to the direction movement (Fig. 6 C). Higher magnification views of the nucleation-based reaction show a high concentration of branched filaments directly behind the bacteria (Fig. 6 D). In contrast, in the elongation reaction filaments make extensive lateral contacts with the bacterial surface, but very few filaments are localized behind it (Fig. 6 E).

Because Arp2/3 has previously been considered central to *L. monocytogenes* propulsion, we took several steps to test if bundling-mediated elongation is truly independent of nucleation by Arp2/3. We performed a dose–response analysis of CA inhibition for the nucleation phase (step 2) and elongation phase (step 3) of our reaction (Fig. 7 A). The Arp2/3-dependent nucleation phase was sensitive to CA inhibition with an IC50 of ∼0.5 μM, whereas CA did not inhibit the fascin-dependent elongation step at concentrations tested up to 15 μM. Second, we tested the effect of a nonhydrolyzable ATP analogue, adenosine 5′-(β,γ-imido)triphosphate (AMPPNP; Fig. 7 B). AMPPNP inhibits nucleation by the Arp2/3 complex by blocking an activation step, but has no effect on the association of Arp2/3 with ActA (Dayel et al., 2001). In that experiment, AMPPNP blocked Arp2/3-dependent nucleation when present at 50-fold molar excess of AMPPNP over ATP, whereas actin polymerization in the first 2 min was not affected by the nucleotide in solution. After that, ATP bound to actin exchanges with nucleotide in solution and further polymerization is inhibited (Selden et al., 1999). In the *Listeria* assay, AMPPNP inhibited cloud formation with an IC50 of ∼0.75 μM which, under these assay conditions, is in 30-fold molar excess of ATP in solution in the nucleation step and 60-fold excess in the elongation step. In the three-step assay, we normally can readily detect cloud formation within the first 60–90 s after Arp2/3 and actin are introduced into the chamber in step 2. Therefore, inhibition of cloud formation by AMPPNP is likely due to inhibition of Arp2/3 activation. In contrast, elongation was insensitive to AMPPNP up to 4 mM. Each of these results, as well as the absence of branched filaments in the

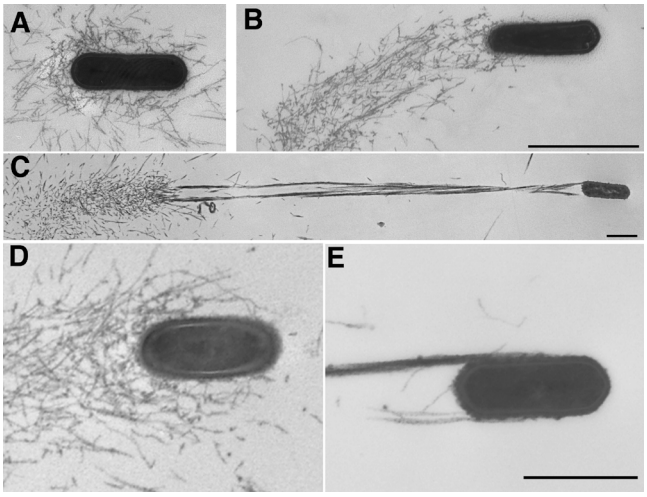

Figure 6. **Thin-section electron micrographs showing segregation of actin filament organization by experimentally separating nucleation-driven propulsion from elongation-driven propulsion.** (A) Branched actin cloud generated by Arp2/3 and actin alone. (B) Branched actin comet tail generated by motility during the Arp2/3-mediated nucleation phase (corresponding to step 2 of Fig. 3). (C) Comet tails after fascin-dependent elongation-driven motility (corresponding to step 3 of Fig. 3). (D) Comet tail organization generated by the nucleation reaction. (E) Comet tail organization generated by the elongation reaction. Bars, 1 μm. Bar in B applies to A and B. Bar in E applies to D and E.

fascin-mediated reaction, argue that the fascin-mediated elongation phase, once initiated, is independent of Arp2/3-nucleating activity. To test if Arp2/3 might play a role other than nucleation in the elongation phase, we introduced Arp2/3 labeled with a green fluorophore in step 2 and assessed its localization after elongation with fascin in step 3 (Fig. 7 C). Arp2/3 localized to the portion of the comet tail assembled in the nucleation phase (step 2), but was not detected in the tail extension generated in the presence of fascin and CA in step 3 nor at the bacterial surface.

In all of the previous experiments, motility was inferred from morphology by the appearance of a long segment of red actin extending away from the green tail assembled in the presence of Arp2/3. To directly measure motility, we used time-lapse phase-contrast or differential interference contrast imaging in the same three-step assay in perfusion chambers. When bacteria are preincubated in cytosol and step 3 contains fascin and actin, the bacteria move at nearly constant rates (~2 μm/min) for 6 min before they start to decelerate (Fig. 8, A and B). The deceleration is due to depletion of actin or fascin from solution because refreshing the perfusion mixture promoted a new round of elongation on a subset of the bacteria (unpublished data). In contrast, when step 3 contains actin alone, the bacteria move only a short distance (to a maximum of 4 μm) before they stop (Fig. 8, A and B). In either the presence of fascin + actin or actin alone, bacteria rarely detached from the comet tail. From these experiments, we conclude that an actin cross-linking protein is required for persistent movement in the absence of Arp2/3, but actin alone is sufficient for a short burst of motility.

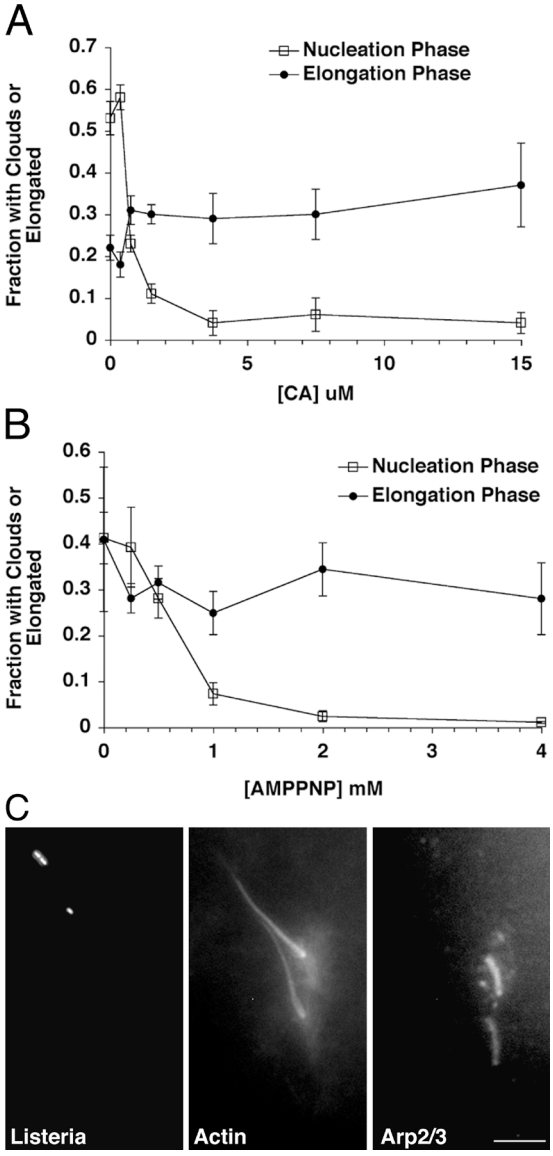

Figure 7. **The fascin-mediated elongation phase is independent of Arp2/3-nucleating activity.** (A) CA inhibits Arp2/3-dependent nucleation, but does not affect fascin-mediated elongation. (B) AMPPNP inhibits Arp2/3-dependent nucleation, but does not affect fascin-mediated elongation. Each point in A and B represents the average of at least 66 bacteria from two experiments ± SD. (C) Arp2/3 localizes to the portion of the comet tail assembled during the nucleation phase, but is not found on the tail assembled during elongation or at the bacterial surface. Bar, 10 μm.

To further characterize the nucleation- and elongation-driven reactions, we compared the rates of *L. monocytogenes* motility of all our different reactions as a function of G-actin concentration (Fig. 9). First, we tested motility in the presence of Arp2/3, VASP, capping protein, and actin in the absence of a cytosol preincubation. This is similar to the defined system for *L. monocytogenes* motility (Loisel et al., 1999), but it lacks profilin and cofilin so the F-actin is not depolymerizing or recycling, and the concentration of G-actin is not buffered. Under these conditions, *L. monocytogenes* move at a rate of 0.5–1 μm/min regardless of the G-actin concentration (1–16 μM). When this mixture is replaced

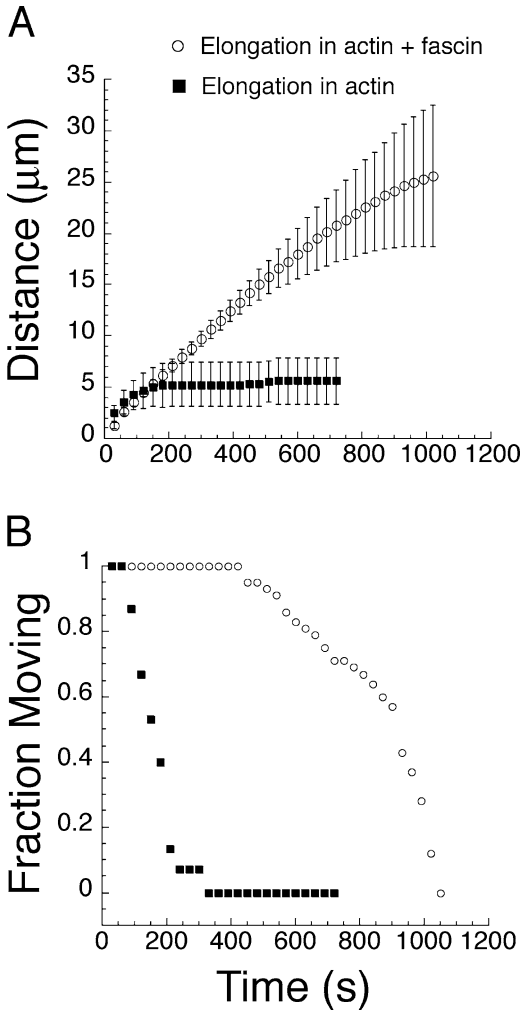

Figure 8. ***L. monocytogenes* motility in the fascin-dependent elongation phase.** (A) Distance traveled over time in the presence or absence of fascin. Each point is the average of at least 57 bacteria ± SD. Every bacterium is included in each time interval, even if it stopped moving at an earlier time. (B) The fraction of the total population moving over time in the presence or absence of fascin.

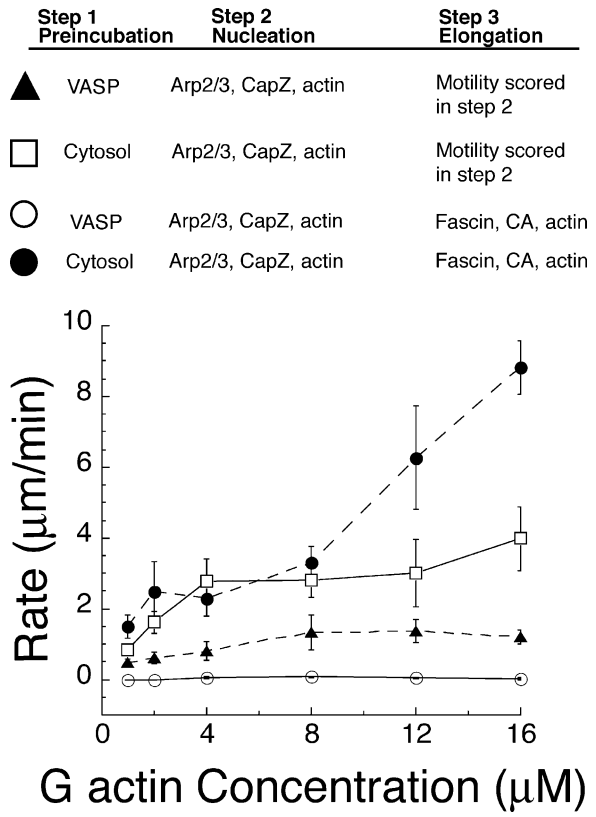

Figure 9. **Rates of *L. monocytogenes* motility as a function of G-actin concentration under nucleation and elongation conditions.** Bacteria were preincubated in either VASP or brain cytosol (step 1). To initiate motility, the preincubation solution was replaced with Arp2/3, actin, and capping protein (step 2). For motility in the absence of Arp2/3, the nucleating solution in step 2 was replaced with a solution containing actin, fascin, and CA (step 3). Motility rates in the Arp2/3-dependent reaction were analyzed in step 2. Rates in the fascin-dependent elongation reaction were analyzed in step 3. Each point is the average of at least 30 bacteria from three separate experiments ± SD.

with fascin and actin, all movement stops. If, instead, the bacteria are preincubated with cytosol and then mixed with Arp2/3, capping protein, and actin (equivalent to step 2 in our three-step reaction), they move faster than in the defined system. The rate depends on actin concentration at low G-actin concentrations and plateaus above 4 μM. *L. monocytogenes* move faster still when this mixture is replaced with fascin and actin (equivalent to step 3 in the three-step reaction), and the rate depends on the actin concentration at all of the concentrations tested. Thus, elongation-based motility is faster than Arp2/3-dependent motility. The elongation reaction absolutely requires one or more unknown factors that can bind to the bacterial surface, and these factors facilitate Arp2/3-dependent motility.

Discussion

L. monocytogenes motility can be experimentally separated into an Arp2/3-dependent nucleation phase and an Arp2/3-independent elongation phase. Elongation-mediated propulsion, unlike propulsion mediated by frequent nucleation, requires an actin-bundling protein and an unknown factor that associates with the bacterial surface. Each biochemical mechanism generates a distinct comet tail structure. The additional biochemical requirements, alternative filament organization, and different dependence of rate on G-actin concentration all suggest that elongation-driven motility is not a simple continuation of the Arp2/3-mediated reaction. We surmise that the mechanical mechanisms for generating force likely differ in the two reactions.

Although the biophysical mechanism by which actin polymerization drives propulsion is not known for Arp2/3-dependent motility, it has been subject to extensive theoretical analysis (Merz and Higgs, 2003; Mogilner and Oster, 2003b; Upadhyaya and van Oudenaarden, 2003). Growing barbed ends near the bacterial surface are thought to either push or squeeze the bacteria forward or prevent it from diffusing backward. Comet tails generated by frequent Arp2/3-dependent nucleation contain a number of filaments directly behind the bacteria that are properly positioned to push as they grow. It is not clear whether these models can account

for force production in the elongation-mediated reaction where very few filaments are localized behind bacteria. During elongation, the vast majority of filaments are bundled and bound to the sides of the bacteria. Despite the fact that these filaments are not positioned to push or prevent backward diffusion in the manner predicted by the elastic Brownian ratchet (Mogilner and Oster, 2003a), bacteria in fact move faster under elongation conditions than nucleation conditions. One reason for faster motility during elongation might be the absence of friction between the comet tail and the bacteria that normally limits the rate of motility in the presence of Arp2/3. Deformation of liposomes coated with ActA revealed a pulling force at the rear that retards forward movement (Giardini et al., 2003). Under elongation-driven conditions there are no filaments behind the bacteria, so this pulling force may not exist. Thus, actin polymerization becomes rate limiting.

The implication of the structural data is that the elongation reaction generates mechanical force using filaments bound to the bacterial surface along the side of the filament. If a myosin motor were attached to the surface of the bacteria, it could use ATP hydrolysis to walk up the laterally attached bundles. However, the elongation reaction is resistant to high concentrations of the nonhydrolyzable ATP analogue AMPPNP. In addition, we have not detected a myosin using a pan-myosin antibody in fractions enriched in the *Listeria*-bound factor, which is required for elongation, on Western blots. Therefore, we consider a myosin-based transport mechanism for *L. monocytogenes* propulsion highly unlikely even for our Arp2/3-independent elongation reaction.

The strong requirement for a bundling protein provides clues as to the biophysical mechanism of the elongation reaction. One possible function of fascin is simply to establish a stable base such that force generated by actin polymerization can be used for useful work. In the absence of a bundling protein, filaments longer than 30–150 nm would simply buckle under a load, and thus could not generate force in the Mogilner and Oster Brownian ratchet model (Mogilner and Oster, 1996). Arp2/3 repeatedly supplies a new population of branched, short filaments that are capable of exerting force which might explain the lack of a requirement for a bundling protein when it is present.

An alternative interpretation of the fascin requirement is that bundling plays a more direct role in force production. Bundling the filaments comprising the hollow cylinder assembled by the elongation reaction could squeeze the bacteria forward. Compressive forces are considered to drive motility in an elastic model of *L. monocytogenes* propulsion (Gerbal et al., 2000), and such forces have been shown to be exerted on ActA-coated liposomes (Giardini et al., 2003; Upadhyaya et al., 2003). We would favor such a mechanism if the comet tail assembled by the elongation showed any sign of collapsing behind the bacteria, but this is not seen. As an alternative, we consider a Brownian ratchet in which diffusion is rectified by bundling (Fig. 10). In this model, we hypothesize that individual filaments form weak attachments to the bacterial surface, but bundling of filaments is incompatible with attachment to the surface. Therefore, as bundling proceeds to form energetically favorable bonds, the bacterium diffuses forward to form favorable bonds with individual filaments growing in front of it. The total number of bonds in the system is maximized by forward movement of the bacterium. We have found that other actin cross-linking proteins such as fimbrin, α-actinin, and filamin can substitute for fascin in the elongation reaction. Perhaps comparing quantitative differences between the different bundling factors to formal models of force generation, in addition to identification of the unknown factor, can help distinguish the mechanism of elongation-driven motility.

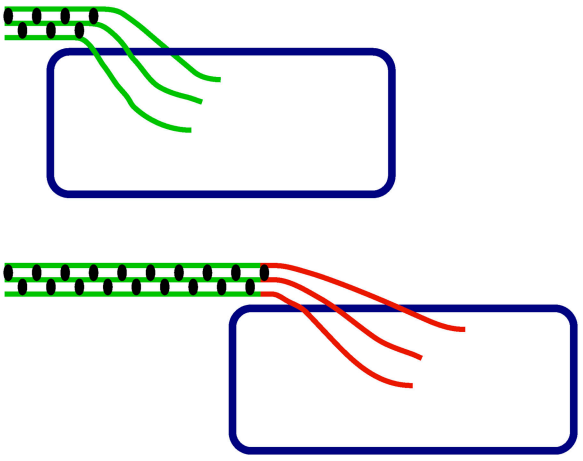

Figure 10. **A Brownian ratchet model for bundling-mediated motility of *L. monocytogenes*.** Individual filaments form weak attachments with the bacterial surface. However, incorporation of filaments into bundles is incompatible with their binding to the bacterial surface. Moving the bacteria to the right maximizes the number of favorable bonds because it can attach to growing individual filaments while leaving bundled filaments behind it. The bacteria is blue. Green lines represent actin and red lines newly polymerized actin. Bundling proteins are represented as black ovals.

Beyond its biophysical interest, is the elongation reaction physiologically significant for *L. monocytogenes* biology? Our EM of *L. monocytogenes* in infected cells and crude extracts suggests that physiological comet tails are typically surrounded by a sheath of bundled actin filaments. Polarization microscopy observations (Zhukarev et al., 1995) and EM of *L. monocytogenes* in protrusions (Sechi et al., 1997) are consistent with the presence of such a sheath. Our three-step assay suggests that this sheath is generated by the elongation reaction, whereas the gel inside the sheath is generated by Arp2/3-driven nucleation. The sheath might provide extra force for propulsion or may simply stiffen the comet tail. The morphology of comet tails we observed in the Arp2/3-driven and elongation reactions shows that the persistence length of the fascin-bundled sheath is much longer than the Arp2/3 cross-linked, branched gel, as expected from their structures. In infected cells, *L. monocytogenes* motility ceases and protrusions withdraw when the cells are injected with fragments of α-actinin (Dold et al., 1994). Therefore, comet tail stiffness might be important when *L. monocytogenes* needs to deform the plasma membrane in a filopodium-like protrusion, where the stiffness of the plasma membrane and submembranous cortex is opposing the stiffness of the comet tail. Unidirectional persistence of motility might also be important for the infectious life cycle because the effi-

ciency of bacterial invasion between cells has been shown to correlate more with the unidirectional persistence of bacterial motility than with motility rate (Monack and Theriot, 2001). Testing the physiological significance of the elongation reaction will require depletion experiments in cells. Depletion of all bundling proteins in cells will be difficult, so the best approach may be to identify the missing *Listeria*-bound factor(s) that are required for the elongation reaction, and to test the effect of depleting it on *L. monocytogenes* biology. Identification of this factor(s) would also help elucidate the physiological process *L. monocytogenes* is hijacking to perform the elongation reaction.

Materials and methods

Protein purification

Actin (Pardee and Spudich, 1982) and CapZ (Casella and Cooper, 1991) were purified from rabbit skeletal muscle as described. Arp2/3 was purified from bovine brain as described previously (Egile et al., 1999). Recombinant, 6His-tagged VASP (a gift from Frederick Southwick, University from Florida College of Medicine, Gainesville, FL) expressed in Sf9 cells with baculovirus was purified on nickel chelating resin followed by gel filtration on a Superdex™ 200 column. Recombinant fascin (a gift from Pierre McCrea, M.D. Anderson Cancer Center, Houston, TX) was purified as a thioredoxin fusion protein from bacteria (Tao et al., 1996) by conventional chromatography. Bacterial extracts were prepared in 20 mM Pipes, pH 6.8, 50 mM KCl, and 5 mM β-mercaptoethanol (β-Me). The extract was centrifuged for 1 h at 108,000 *g*. The supernatant was passed through a 2× 5-ml DEAE HiTrap™ column linked in tandem that flowed into a 5-ml S HiTrap™ column (Amersham Biosciences). The flow-through from these linked columns was dialyzed against 20 mM MES, pH 6.0, and 5 mM β-Me, applied to a Mono S 5/5 column, and eluted with a 20-ml gradient to 300 mM KCl in the dialyzing buffer. Fascin–thioredoxin eluted around 75–120 mM KCl. Fascin-positive fractions were gel filtered on a 16/60 Superdex™ 200 column equilibrated in 20 mM Pipes, pH 6.8, 100 mM KCl, and 5 mM β-Me. Recombinant fimbrin was a gift from Paul Matsudaira (MIT, Cambridge, MA). To purify recombinant fimbrin from bacteria, lysates were prepared in 20 mM Tris, pH 8.0, and 5 mM β-Me. The 108,000 *g* supernatant was precipitated with 30–70% ammonium sulfate and the pellet was resuspended in 20 mM Tris, pH 8.0, 50 mM KCl, and 5 mM β-Me. After dialyzing against the same buffer, the sample was applied to a 2× 5-ml DEAE HiTrap™ column. The column was eluted with a 15-volume gradient to 500 mM KCl in the same buffer. Fractions containing fimbrin were precipitated with 70% ammonium sulfate, pelleted, resuspended in 20 mM Tris, pH 7.4, and 5 mM β-Me, and applied to a 16/60 Superdex™ 200 column equilibrated in 20 mM Tris, pH 7.4, 100 mM KCl, and 5 mM β-Me. Positive fractions were pooled, diluted fourfold in 20 mM Tris, pH 7.4, and applied to a Mono Q 5/5 column equilibrated in 20 mM Tris, pH 7.4, and 5 mM β-Me. The column was eluted with a 20-ml gradient to 400 mM KCl in the same buffer. Fimbrin eluted between 180 and 200 mM KCl. α-Actinin and filamin were purified from chicken gizzard as described previously (Feramisco and Burridge, 1980).

Protein labeling

Actin was labeled with either tetramethylrhodamine (TMR) or Alexa® 488 *N*-hydroxysuccinimide esters as described previously (Kellogg et al., 1988), except 0.6 M KI was used for the first depolymerization step after the labeling reaction. Arp2/3 was labeled with Alexa® 488 maleimide as described previously (Zalevsky et al., 2001). Working stocks of labeled G-actin were prepared by mixing 2 μl of a 6-mg/ml solution of G-actin labeled 1:2 to 1:3 (fluorophores/actin) with 25 μl unlabeled G-actin at 6 mg/ml.

Motility assays

L. monocytogenes were labeled with DAPI, killed with iodoacetamide, and stored at −80°C as described previously (Welch and Mitchison, 1998). Perfusion chambers were assembled from glass slides, glass coverslips, and double-stick tape. Bacteria were diluted into assay buffer (20 mM Pipes, pH 6.8, 75 mM KCl, 1 mM $MgCl_2$, 1 mM ATP, and 5 mM β-Me), introduced into the chamber, and absorbed to the glass for 10 min.

Two-step assays. For two-step reactions in total cytosol, 100,000 *g* brain supernatants were diluted 1:5 in assay buffer, and alexa® 488–labeled G-actin, from a working stock solution described above, was added to 5 μM. After 5 min, the solution in the chamber was replaced with the same dilution of cytosol, but with 5 μM TMR-labeled actin and 5 μM CA-GST (a gift from Terry Lechler and Rong Li, Harvard Medical School, Boston, MA).

Three-step assays. 100,000 *g* brain supernatants were diluted 1:5 in assay buffer and introduced into perfusion chambers containing absorbed bacteria (step 1). After a 10-min incubation at 4°C, the chamber was rinsed twice with one chamber volume each of assay buffer before introducing a solution containing 0.3 μM Arp2/3, 5 μM Alexa® 488–labeled actin, and 2 nM CapZ (step 2) in assay buffer. After 5 min, the chamber was washed twice with assay buffer followed by a solution containing 5 μM TMR-labeled actin, 5 μM CA-GST, and an appropriate dilution of fractions from bovine brain (step 3) or 1 μM recombinant fascin, fimbrin, α-actinin, or filamin. Extension of the comet tail under elongation conditions in step 3 was assessed after 5 min.

Images of the reactions were acquired on a microscope (model E800; Nikon) equipped with a cooled CCD camera (Princeton Instruments) using MetaMorph® acquisition software (Universal Imaging Corp.). Images were taken with a 60× 1.4 NA oil objective.

Purification of fascin from bovine brain

Freshly isolated bovine calf brains were homogenized in a Waring type blender in 100 ml buffer A (20 mM Pipes, pH 6.8, 25 mM KCl, 2 mM $MgCl_2$, 5 mM β-Me, and 0.2 mM PMSF) per 100 g of tissue. Fascin was purified from a 100,000 *g* supernatant of bovine brain by passing the material over S-Sepharose HP (Amersham Biosciences) in buffer A. The column was eluted with a gradient from 0 to 350 mM KCl in buffer A. The flow-through contained all the activity required for step 3 and was used for purification of fascin. The bound material contained all nucleating activity and was used to purify Arp2/3. The S flow-through was dialyzed into buffer B (buffer A, but with 20 mM MES, pH 6.0) and was reapplied to the S column in buffer B and eluted with a 15-column volume gradient from 0 to 350 mM KCl. Active fractions were desalted back into buffer A on Sephadex G-25 and were applied to a heparin sulfate column equilibrated in buffer A. The column was eluted with a 15-column volume gradient from 0 to 750 ml KCl. Active fractions were dialyzed into buffer A and added to a threefold protein mass excess of phalloidin-stabilized actin filaments. The sample was incubated on ice for 60 min before collecting the actin filaments and associated proteins by centrifugation at 100,000 *g* for 30 min in a TLA100.3 rotor (Beckman Coulter). The pellet was washed 2× in buffer A, and was then homogenized in 1 M KCl in buffer A. The actin was pelleted and the supernatant was desalted on Sephadex G-25 into buffer A before being applied to a 1-ml Q HiTrap™ column equilibrated in buffer A. Fascin flows through the column under these conditions.

CA and AMPPNP inhibition of Arp2/3-nucleating activity

Listeria absorbed to glass in perfusion chambers were preincubated in cytosol for 10 min, and the chamber was washed twice as above. To assess inhibition of Arp2/3-dependent nucleation, the chamber was filled with 0.3 μM Arp2/3, 2 nM capping protein, and 5 μM Alexa® 488–labeled actin in assay buffer containing varying concentrations of CA-GST. Nucleation of clouds and comet tails was assessed by fluorescence microscopy after 10 min. CA inhibition of elongation was determined by adding varying amounts of CA-GST to the elongation reaction solution containing 1 μM fascin and 5 μM TMR-labeled actin. Elongation was assessed by fluorescence microscopy after 5 min. Inhibition by AMPPNP was performed in essentially the same way, except that ATP was omitted from the assay buffer during the step in which AMPPNP was used. Therefore, the only ATP in the buffer at that time comes from the actin and Arp2/3 solutions. For each concentration of CA-GST or AMPPNP, three random 40× fields were photographed in two separate experiments, and the average number of bacteria with associated clouds or tails or elongated tails was determined.

Motility rates

The rate of elongation in the presence and absence of fascin was determined in perfusion chambers in a three-step reaction as described above. After preincubation in cytosol, initiation in Arp2/3, actin, and capping protein, and a buffer wash, the chamber was filled with assay buffer containing 5 μM CA-GST and 5 μM actin with or without 1 μM fascin. Motility was recorded by time-lapse microscopy during this third step using either phase-contrast or differential interference contrast optics acquiring an image every 30 s. Rates and distances were determined using the "Track Objects" feature on MetaMorph®.

Motility rates as a function of G-actin concentration were determined in perfusion chambers in either a two- or three-step reaction. Bacteria were

either preincubated in cytosol diluted in assay buffer as described above, or in 2 μM recombinant VASP in assay buffer with 4 mg/ml casein. After preincubation and washing, reactions were initiated with Arp2/3, capping protein, and the indicated concentration of G-actin. To determine rates in the presence of Arp2/3, motility was assessed in this second step. To determine rates in the elongation phase, the initiating solution was replaced after a 5-min incubation with fascin, CA, and the indicated concentration of G-actin.

Infection of cultured cells

For EM, PtK cells were cultured on aclar plastic. Discs of aclar were glow discharged, coated with polylysine, and washed extensively with water before the addition of PtK cells. After an overnight incubation, PtK cells were infected with *L. monocytogenes* for 90 min, washed into fresh media containing 50 μg/ml gentamicin, and incubated at 37°C for 4 h before fixation and processing for EM.

For immunofluorescence, BSC-1 cells or XTC cells were cultured on polylysine-coated glass coverslips, infected with *L. monocytogenes* for 3 h, washed into media containing 50 μg/ml gentamicin, and incubated at 37°C for an additional 4 h. The cells were fixed in methanol and costained for fascin using an anti-fascin mAb (clone 55K-2; DakoCytomation), and for actin using an anti-actin rabbit pAb (Sigma-Aldrich).

Electron microscopy

Infected PtK cells were rinsed twice with PBS and permeabilized for 3 min with 0.1% Triton X-100 in 20 mM Pipes, pH 6.8, and 100 mM KCl. The cells were then fixed with 50 mM lysine and 3% glutaraldehyde in 50 mM cacodylate, pH 7.0, for 5 min, and then with 3% glutaraldehyde in cacodylate buffer. Samples were postfixed after three rinses in cacodylate with 1% osmium and 0.8% $K_3Fe(CN)_6$ in cacodylate buffer for 15 min on ice. After three rinses in cacodylate and two rinses in water, samples were stained with 1% uranyl acetate for at least 2 h. Samples were rinsed twice with water and then were dehydrated with an ethanol series from 35 to 100% ethanol while progressively lowering the temperature from 4 to −40°C. Samples were embedded in Epon-Araldite and were thin sectioned.

For in vitro EM, motility reactions were performed in perfusion chambers consisting of a glass slide and an aclar coverslip. Bacteria were incubated in the chamber with the coverslip down to encourage absorption to the plastic coverslip. Motility reactions were performed as described above and were then fixed and processed for thin-section EM as described above.

We thank Terry Lechler, Rong Li, Paul Matsudaira, Pierre McCrea, and Fred Southwick for reagents. Mass spectrometry was performed by Jim Lee. We are grateful to members of the Mitchison lab and especially to Aaron Straight for insights and helpful discussions. Mimi Shirasu-Hiza offered needed advice in the cold room. We thank Zach Perlman and are especially grateful to Guillaume Charas for discussing mechanisms of *Listeria* propulsion.

W.M. Brieher acknowledges the support of the Helen Hay Whitney Foundation. This work was supported by National Institutes of Health grant GM 48027.

Submitted: 7 November 2003
Accepted: 24 March 2004

References

Bernheim-Groswasser, A., S. Wiesner, R.M. Golsteyn, M.F. Carlier, and C. Sykes. 2002. The dynamics of actin-based motility depend on surface parameters. *Nature.* 417:308–311.

Cameron, L.A., P.A. Giardini, F.S. Soo, and J.A. Theriot. 2000. Secrets of actin-based motility revealed by a bacterial pathogen. *Nat. Rev. Mol. Cell Biol.* 1:110–119.

Cameron, L.A., T.M. Svitkina, D. Vignjevic, J.A. Theriot, and G.G. Borisy. 2001. Dendritic organization of actin comet tails. *Curr. Biol.* 11:130–135.

Casella, J.F., and J.A. Cooper. 1991. Purification of cap Z from chicken skeletal muscle. *Methods Enzymol.* 196:140–152.

Dabiri, G.A., J.M. Sanger, D.A. Portnoy, and F.S. Southwick. 1990. *Listeria monocytogenes* moves rapidly through the host-cell cytoplasm by inducing directional actin assembly. *Proc. Natl. Acad. Sci. USA.* 87:6068–6072.

Dayel, M.J., E.A. Holleran, and R.D. Mullins. 2001. Arp2/3 complex requires hydrolyzable ATP for nucleation of new actin filaments. *Proc. Natl. Acad. Sci. USA.* 98:14871–14876.

Dold, F.G., J.M. Sanger, and J.W. Sanger. 1994. Intact α-actinin molecules are needed for both the assembly of actin into the tails and the locomotion of *Listeria monocytogenes* inside infected cells. *Cell Motil. Cytoskeleton.* 28:97–107.

Egile, C., T.P. Loisel, V. Laurent, R. Li, D. Pantaloni, P.J. Sansonetti, and M.F. Carlier. 1999. Activation of the CDC42 effector N-WASP by the *Shigella* flexneri IcsA protein promotes actin nucleation by Arp2/3 complex and bacterial actin-based motility. *J. Cell Biol.* 146:1319–1332.

Feramisco, J.R., and K. Burridge. 1980. A rapid purification of α-actinin, filamin, and a 130,000-dalton protein from smooth muscle. *J. Biol. Chem.* 255: 1194–1199.

Gerbal, F., P. Chaikin, Y. Rabin, and J. Prost. 2000. An elastic analysis of *Listeria monocytogenes* propulsion. *Biophys. J.* 79:2259–2275.

Giardini, P.A., D.A. Fletcher, and J.A. Theriot. 2003. Compression forces generated by actin comet tails on lipid vesicles. *Proc. Natl. Acad. Sci. USA.* 100: 6493–6498.

Kellogg, D.R., T.J. Mitchison, and B.M. Alberts. 1988. Behaviour of microtubules and actin filaments in living *Drosophila* embryos. *Development.* 103:675–686.

Kocks, C., and P. Cossart. 1993. Directional actin assembly by *Listeria monocytogenes* at the site of polar surface expression of the actA gene product involving the actin-bundling protein plastin (fimbrin). *Infect. Agents Dis.* 2:207–209.

Lewis, A.K., and P.C. Bridgman. 1992. Nerve growth cone lamellipodia contain two populations of actin filaments that differ in organization and polarity. *J. Cell Biol.* 119:1219–1243.

Loisel, T.P., R. Boujemaa, D. Pantaloni, and M.F. Carlier. 1999. Reconstitution of actin-based motility of *Listeria* and *Shigella* using pure proteins. *Nature.* 401: 613–616.

Mallavarapu, A., and T. Mitchison. 1999. Regulated actin cytoskeleton assembly at filopodium tips controls their extension and retraction. *J. Cell Biol.* 146: 1097–1106.

May, R.C., M.E. Hall, H.N. Higgs, T.D. Pollard, T. Chakraborty, J. Wehland, L.M. Machesky, and A.S. Sechi. 1999. The Arp2/3 complex is essential for the actin-based motility of *Listeria monocytogenes*. *Curr. Biol.* 9:759–762.

Merz, A.J., and H.N. Higgs. 2003. *Listeria* motility: biophysics pushes things forward. *Curr. Biol.* 13:R302–R304.

Mogilner, A., and G. Oster. 1996. Cell motility driven by actin polymerization. *Biophys. J.* 71:3030–3045.

Mogilner, A., and G. Oster. 2003a. Force generation by actin polymerization II: the elastic ratchet and tethered filaments. *Biophys. J.* 84:1591–1605.

Mogilner, A., and G. Oster. 2003b. Polymer motors: pushing out the front and pulling up the back. *Curr. Biol.* 13:R721–R733.

Monack, D.M., and J.A. Theriot. 2001. Actin-based motility is sufficient for bacterial membrane protrusion formation and host cell uptake. *Cell. Microbiol.* 3:633–647.

Mullins, R.D., J.A. Heuser, and T.D. Pollard. 1998. The interaction of Arp2/3 complex with actin: nucleation, high affinity pointed end capping, and formation of branching networks of filaments. *Proc. Natl. Acad. Sci. USA.* 95: 6181–6186.

Pardee, J.D., and J.A. Spudich. 1982. Purification of muscle actin. *Methods Enzymol.* 85:164–181.

Pollard, T.D., and G.G. Borisy. 2003. Cellular motility driven by assembly and disassembly of actin filaments. *Cell.* 112:453–465.

Portnoy, D.A., V. Auerbuch, and I.J. Glomski. 2002. The cell biology of *Listeria monocytogenes* infection: the intersection of bacterial pathogenesis and cell-mediated immunity. *J. Cell Biol.* 158:409–414.

Sechi, A.S., J. Wehland, and J.V. Small. 1997. The isolated comet tail pseudopodium of *Listeria monocytogenes*: a tail of two actin filament populations, long and axial and short and random. *J. Cell Biol.* 137:155–167.

Selden, L.A., H.J. Kinosian, J.E. Estes, and L.C. Gershman. 1999. Impact of profilin on actin-bound nucleotide exchange and actin polymerization dynamics. *Biochemistry.* 38:2769–2778.

Svitkina, T.M., and G.G. Borisy. 1999. Arp2/3 complex and actin depolymerizing factor/cofilin in dendritic organization and treadmilling of actin filament array in lamellipodia. *J. Cell Biol.* 145:1009–1026.

Svitkina, T.M., E.A. Bulanova, O.Y. Chaga, D.M. Vignjevic, S. Kojima, J.M. Vasiliev, and G.G. Borisy. 2003. Mechanism of filopodia initiation by reorganization of a dendritic network. *J. Cell Biol.* 160:409–421.

Tao, Y.S., R.A. Edwards, B. Tubb, S. Wang, J. Bryan, and P.D. McCrea. 1996. β-Catenin associates with the actin-bundling protein fascin in a noncadherin complex. *J. Cell Biol.* 134:1271–1281.

Taunton, J., B.A. Rowning, M.L. Coughlin, M. Wu, R.T. Moon, T.J. Mitchison, and C.A. Larabell. 2000. Actin-dependent propulsion of endosomes and ly-

sosomes by recruitment of N-WASP. *J. Cell Biol.* 148:519–530.

Theriot, J.A., and T.J. Mitchison. 1991. Actin microfilament dynamics in locomoting cells. *Nature.* 352:126–131.

Theriot, J.A., T.J. Mitchison, L.G. Tilney, and D.A. Portnoy. 1992. The rate of actin-based motility of intracellular *Listeria monocytogenes* equals the rate of actin polymerization. *Nature.* 357:257–260.

Tilney, L.G., and D.A. Portnoy. 1989. Actin filaments and the growth, movement, and spread of the intracellular bacterial parasite, *Listeria monocytogenes*. *J. Cell Biol.* 109:1597–1608.

Tilney, L.G., D.J. DeRosier, A. Weber, and M.S. Tilney. 1992. How *Listeria* exploits host cell actin to form its own cytoskeleton. II. Nucleation, actin filament polarity, filament assembly, and evidence for a pointed end capper. *J. Cell Biol.* 118:83–93.

Upadhyaya, A., and A. van Oudenaarden. 2003. Biomimetic systems for studying actin-based motility. *Curr. Biol.* 13:R734–R744.

Upadhyaya, A., J.R. Chabot, A. Andreeva, A. Samadani, and A. van Oudenaarden. 2003. Probing polymerization forces by using actin-propelled lipid vesicles. *Proc. Natl. Acad. Sci. USA.* 100:4521–4526.

Vignjevic, D., D. Yarar, M.D. Welch, J. Peloquin, T. Svitkina, and G.G. Borisy. 2003. Formation of filopodia-like bundles in vitro from a dendritic network. *J. Cell Biol.* 160:951–962.

Welch, M.D., and T.J. Mitchison. 1998. Purification and assay of the platelet Arp2/3 complex. *Methods Enzymol.* 298:52–61.

Welch, M.D., A. Iwamatsu, and T.J. Mitchison. 1997. Actin polymerization is induced by Arp2/3 protein complex at the surface of *Listeria monocytogenes*. *Nature.* 385:265–269.

Wiesner, S., E. Helfer, D. Didry, G. Ducouret, F. Lafuma, M.F. Carlier, and D. Pantaloni. 2003. A biomimetic motility assay provides insight into the mechanism of actin-based motility. *J. Cell Biol.* 160:387–398.

Yarar, D., W. To, A. Abo, and M.D. Welch. 1999. The Wiskott-Aldrich syndrome protein directs actin-based motility by stimulating actin nucleation with the Arp2/3 complex. *Curr. Biol.* 9:555–558.

Zalevsky, J., I. Grigorova, and R.D. Mullins. 2001. Activation of the Arp2/3 complex by the *Listeria* acta protein. Acta binds two actin monomers and three subunits of the Arp2/3 complex. *J. Biol. Chem.* 276:3468–3475.

Zhukarev, V., F. Ashton, J.M. Sanger, J.W. Sanger, and H. Shuman. 1995. Organization and structure of actin filament bundles in *Listeria*-infected cells. *Cell Motil. Cytoskeleton.* 30:229–246.